Automation in Construction 107 (2019) 102948

Contents lists available at ScienceDirect

Automation in Construction

journal homepage: www.elsevier.com/locate/autcon

Design framework for the structural analysis of free-form timber plate structures using wood-wood connections

Anh Chi Nguyen*, Petras Vestartas, Yves Weinand

Laboratory for Timber Constructions (IBOIS), École Polytechnique Fédérale de Lausanne, GC H2 711, Station 18, Lausanne CH-1015, Switzerland

ARTICLE INFO

Keywords:
Timber plate structures
Wood-wood connections
Digital fabrication
Finite element method
Semi-rigidity
Spring model

ABSTRACT

Geometrically complex timber plate structures using wood-wood connections are increasingly designed thanks to digital fabrication. Whereas their fabrication has been automated using computer-aided design programming, research focused on the development of automated numerical tools for their structural analysis has been very limited. This paper presents a method to automate the generation of a finite element model for the analysis of structures with a large number of joints. The model is developed taking the example of recently developed double-layered timber plate shells. Vertical displacements obtained with the semi-rigid spring model proposed are in good agreement with experimental tests performed on small-scale prototypes, whereas rigid modelling of the connections highly underestimates displacements of the structure. Semi-rigidity of the connections in translation as well as in rotation was shown to highly influence the model. The generation of the numerical model was successfully automated for large-scale structures.

1. Introduction

Recent advances in information-tool technology have led to the development of computer-numerical-control (CNC)-fabricated wood-wood connections, inspired by traditional woodworking joints [1] . Initially used for timber frame structures, these joints have recently been applied to timber plate structures, formed by the assembly of discrete thin timber plates mutually connected along their edges. Consequently, digital fabrication has allowed the design of timber plate structures with complex geometries. Researchers have investigated various shape topologies such as segmental plate shells (e.g. *ICD/ITKE Research Pavilion 2011* [2] and *Landesgarteschau Exhibition Hall* [3]) and folded plate structures (e.g. *Lausanne Vidy theatre* [4]). Although the assembly of these structures is still carried out manually, both design and fabrication have been successfully automated using computer-aided design (CAD) programming and automatic prefabrication tools. However, limited research has focused on the development of automated tools for the structural analysis of timber structures with complex geometries. A model is needed which could both accurately predict the mechanical behaviour of the structure and be computationally efficient. Numerical models based on the finite element method (FEM) are generally built since analytical solutions can hardly be found for such complex structures. However, simplified models are required as a three-dimensional (3D) modelling would be too computationally expensive due to the large number of 3D solid elements it would involve [5] . Moreover, complex structures composed of a large number of singular shaped panels with different joint parameters require an automatic generation of the model.

This paper presents a design framework for the structural analysis of free-form timber plate structures using wood-wood connections, taking the example of double-layered double-curved timber plate shells recently developed and applied to the Annen head office in Manternach, Luxembourg. Based on an existing framework generating design and fabrication files of double-layered double-curved timber plate shells developed by Robeller et al. [6] , a finite element (FE) model was generated using CAD programming and a custom code in Python programming language. FE models were generated for small- and large-scale structures. Finally, a structural analysis was carried out for small-scale prototypes and results of the numerical model were compared to experimental tests in order to assess the FE model.

2. Literature review

2.1. Timber plate structures and wood-wood connections

The first shell structures using wood-wood connections for the assembly of planar discrete plates consisted of single tab-and-slot joints (e.g. *Serpentine Pavilion 2005* [7] and *Swissbau Pavilion 2005* [8]).

* Corresponding author.
E-mail address: anhchi.nguyen@epfl.ch (A.C. Nguyen).

https://doi.org/10.1016/j.autcon.2019.102948
Received 20 May 2019; Received in revised form 20 August 2019; Accepted 29 August 2019
Available online 10 September 2019

Multiple joints along the edges of timber plates, similar to traditional multiple-dovetail joints used in cabinetmaking, were subsequently developed. After the utilization of 1-plane joints (*ICD/ITKE Research Pavilion* 2010 [9]), 2-plane finger joints were developed at the University of Stuttgart. They were applied in the *ICD/ITKE Research Pavilion 2011* [2,10] and the segmental plate shell of the *Landesgarteschau Exhibition Hall* [3]. Single-degree-of-freedom (1-DOF) joints were finally developed by Robeller [1] . These multiple tab-and-slot joints (MTSJ) are geometrically defined by three angles θ_1, θ_2 and θ_3. These three Bryant angles, *xyz* convention of the Euler angles [11], influence the mechanical behaviour of the joints. MTSJ have a locator feature in addition to their load bearing function. In fact, they define the position of the plates, allowing a fast and direct assembly of all plates without the need for complex and costly formworks. They have the advantage of providing high rotational stiffness in addition to high in-plane shear resistance with resistance to axial forces and out-of-plane shear forces in comparison with finger joints, which are 3-degrees-of-freedom (3-DOFs) joints [1]. These form-fitting joints have been applied to single- and double-layered folded plate structures [12,4] and more recently, a double-layered double-curved timber plate shell structure has been developed [6]. The latter uses through-tenon joints, referred to as MTSJ-TT or as closed-slot joints, developed by Roche et al. [13].

2.2. Automatic geometry generation and digital fabrication

Structures with a large number of geometrically different plates would have been difficult or even impossible to obtain without automation. In fact, digital fabrication allows all unique-shaped parts of the structure to be fabricated and assembled rapidly and precisely. This has been applied in several cases. For the *ICD/ITKE Research Pavilion 2011* of the University of Stuttgart, custom programs were developed to build the digital model and subsequently the CNC machine code for robotic fabrication [2]. For the Pavilion of the Vidy Theatre, Annen head office in Manternach and folded plate structures developed at the Laboratory for Timber Constructions IBOIS (EPFL), custom CAD plugins were developed for an automated digital modelling and fabrication of each structure. They were programmed in Visual C# language and with Rhino® Common Software Development Kit (SDK), using the visual programming software Grasshopper® as a user interface, allowing a realtime preview of the 3D geometry in function of the chosen input design parameters. In the same manner, a digital fabrication tool was developed to generate a 5-axis CNC machine G-code [4,6,14].

2.3. Numerical modelling

Connections between plates often constitute weak points of timber plate structures and substantially influence the behaviour of the structure. In particular, the semi-rigidity of the connections has to be taken into account in the model since simplifications considering the connections as rigid or hinged respectively lead to over- and underestimated displacements [12,14]. In light of this, while plane shell elements are generally used for timber panels, two numerical approaches exist for integral joints: on the one hand, spring elements can be used to model the semi-rigidity of the connections, as previously utilized for finger joints [2,3] and MTSJ-TT in folded plate structures [14]; on the other hand, strips of fictitious material along edges of connected plates can be used, such as developed for glass structures by Bagger [15] and applied to timber folded plate structures by Stitic et al. [14]. In the latter, both numerical models have shown satisfying results applied to folded plate structures compared to experimental testing results. A macro-modelling approach was also applied to timber folded plate structures [14].

Discrepancies exist among researchers concerning the implementation of spring elements. For the *ICD/ITKE Research Pavilion 2011* [2], single springs have been used to connect two nodes at the opposite sides of neighbouring panels with axial springs acting in the direction of the edges of the finger joints. Custom tools have been developed to generate the FE model of the structure made of more than 100 000 finger joints. However, for this model, no comparison with experimental tests has been performed. For the timber folded plate structures studied by Stitic et al. [14], seven springs were distributed along the length of the through-tenon joints with axial, in-plane shear and rotational stiffness implemented. The remaining components of motion were considered rigid by assigning them high stiffness values of 10^9 N/mm and 10^{15} N·mm/° for translational and rotational components respectively. It was shown that increasing the number of joints distributed along the length of the tenons was converging to results in better agreement with experimental results. The same method was applied for a 5×3 boxes prototype of a double-layered timber plate structure using MTSJ-TT [16].

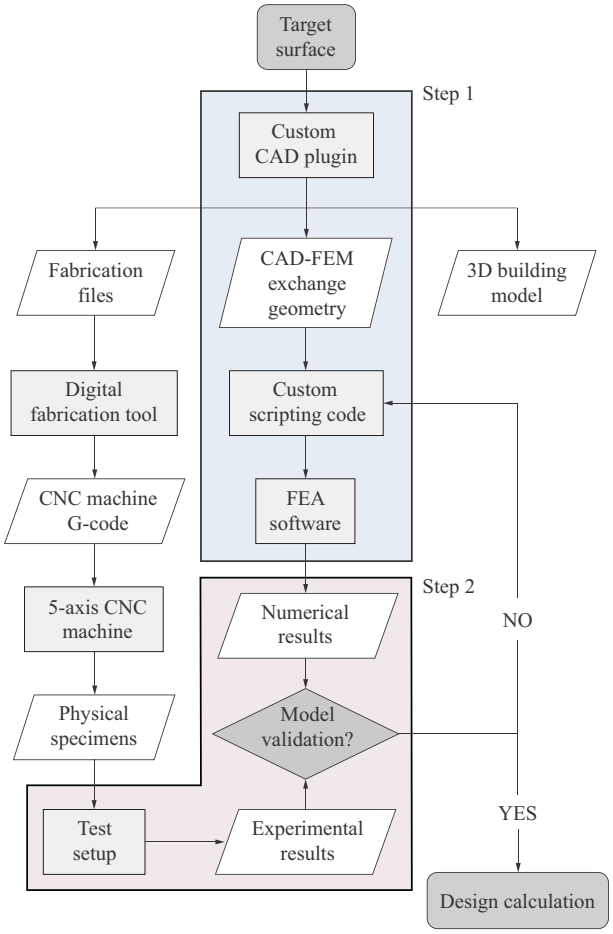

Fig. 1. Design framework proposed. Step 1 consists of the generation of the finite element model and step 2 encompasses investigations on the mechanical behaviour of the structure.

3. Design framework

The design framework proposed to build the FE model for the structural analysis of free-form timber plate structures is presented in Fig. 1 and can be divided into two distinct steps. The final objective is to obtain a numerical model that can lead to accurate design calculations.

The first step consists of the generation of the numerical model. To achieve this step, an exchange geometry is defined in order to import the complex geometry from a CAD software to a finite element analysis (FEA) software, which constitutes a heterogeneous data exchange [17]. Therefore, the computational tool developed for automated digital modelling and fabrication has to include the generation of a third output file, in addition to the 3D building model and the fabrication

files. This simplified geometry is defined according to the numerical model and its assumptions. The model is then built in a FEA software using a custom scripting code. The mechanical behaviour of the structure is then investigated by developing an experimental setup and performing tests on a series of specimens. Results are compared to numerical simulations.

In this paper, the design framework proposed was applied to the case study of the Annen head office. However, the methods presented can be applied to other types of timber plate structures.

4. Case study: Annen head office

4.1. Project description

The first full-scale realization of double-layered and double-curved timber plate shell structures has been constructed for the Annen head office in Manternach, Luxembourg. This project consists of a series of 23 discontinuous and individually shaped shells made of beech laminated veneer lumber (LVL) plates with spans ranging from 22.5 m to 53.7 m and constant height and width of 9 and 6 m respectively. The structures are double-curved and double-layered timber plate shells with design inspired by Eladio Dieste's Gaussian masonry vaults [18]. The project will accommodate a 5800 m^2 facility including a timber prefabrication factory space and offices [6].

4.2. Assembly system

The construction system, developed in Robeller et al. [6], is illustrated in Fig. 2. The shell is made of two interconnected layers of thin timber plates, $H_{i,1}$ and $H_{i,2}$, assembled at their edges by MTSJ-TT connections. Since neighbouring horizontal plates that have to be connected have a large dihedral angle (close to 180°), they are connected with MTSJ-TT through vertical plates $V_{i,1}$ and $V_{i,2}$, themselves connected with dovetail joints. Hexahedra-shaped boxes B_i forming the structure are thus made of four plates: two horizontal ones forming the two layers of the structure and two vertical ones allowing their assembly. The two remaining open sides of each segment are closed by neighbouring segments, vertical plates being shared between every neighbouring segment. All plates are assembled individually along the vector of insertion defined by the remaining DOF of the connection. The interlocking of the plates allows this DOF to be blocked. With this construction system, horizontal plates of each layer are partially in direct contact, allowing a transfer of compressive forces through the layer. Direct and indirect compression zones can therefore be identified [6].

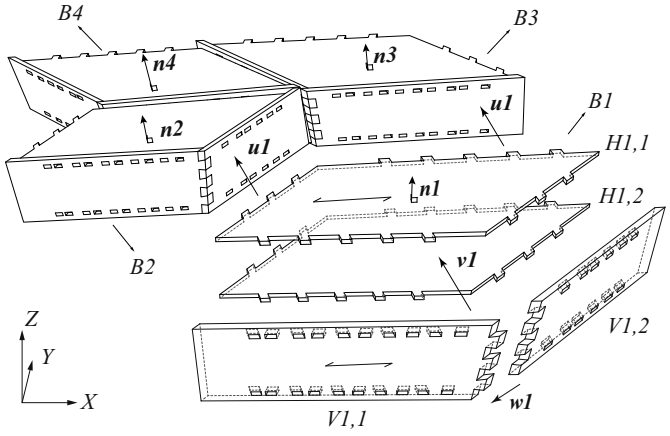

Fig. 2. Construction system of double-layered timber plate shells developed by Robeller et al. [6]. The two layers are formed by horizontal plates $H_{i,1}$ and $H_{i,2}$, which are connected with MTSJ-TT through vertical plates $V_{i,1}$ and $V_{i,2}$. The two horizontal and two vertical plates form hexahedra-shaped boxes B_i.

4.3. Construction material

Pollmeier BauBuche Q panels (with characteristic density ρ_k = 730 kg/m^3) used for the project are 40 mm thick beech LVL panels made of 3 mm thick layers of beech peeled veneers, glued together longitudinally and cross-wised into a panel, unlike BauBuche S panels presenting longitudinal layers only [19]. Since the structure presents connections at each plate's edge, with membrane efforts induced in different directions, crosswise layers panels are preferably chosen. They provide better stiffness properties and higher lateral bending and shear strength. The composition of the 14 veneer layers is |||−||||||−||| (| for longitudinal, − for crosswise veneer layer) [19].

4.4. Fabrication and assembly process

CAD plugins have been developed to automatically design and fabricate double-layered plate shell structures [6]. All panels are cut with a 5-axis CNC milling machine with a 20 mm diameter tool for maximum angles smaller than 45° and with a 25 mm diameter tool for larger tilt angles. All plates forming the boxes are prefabricated and can be manually assembled on-site following a single assembly path. Structures are assembled lying on their longitudinal side and lifted up in one single assembly to their final vertical position. Two screws per edge are added between the horizontal and vertical plates in order to maintain the position of the plates during the assembly of the boxes.

Two prototypes scale 1:1 have been built: a 5 × 3 boxes prototype, fabricated by Annen SA, to study the mechanical behaviour of the structure (see Fig. 3a) [16], and a large-scale prototype of one and a half arches (200 + 100 boxes) with a 24-meter span, fabricated and assembled by Annen SA, to verify the connection details between the arches and to the supports (see Fig. 3b). The geometry of the 5 × 3 boxes prototype, 6.9-meter long, 2.6-meter wide and 0.76-meter high (with a static height of 0.6 m), was defined according to the 24-meter span arch scale 1:1 (see Fig. 4). Fifteen boxes at midspan were extracted and their geometry was simplified to remove the double curvature. All MTSJ-TT were set to a tab length of 72.5 mm and Bryant angles $\theta_1 = 0°$, $\theta_2 = 25°$, $\theta_3 = 0°$.

5. Finite element model generation(Step 1)

5.1. Methodology

As described in Section 3, the first step of the design framework proposed consists of the generation of the FE model. To apply this to our case study, the model was first defined to determine the information required for the CAD-FEM geometry. The latter was then generated and a custom Python scripting code was developed to import this exchange geometry information in the FEA software.

5.1.1. Definition of the finite element model

Several assumptions were taken to model the timber plates and the connections. A numerical model was developed since the proposed mathematical model cannot be calculated analytically due to form complexity, material properties and boundary conditions [14]. Structural analysis of plate shell structures is usually performed with the FEM due to its ease of implementation. Since an exact 3D modelling would have been computationally expensive, simplifications of the model were applied. As the structure can be decomposed in discrete planar continuous elements, plate theory was considered for the mathematical model and plates were modelled as shell elements, as opposed to solid elements, since their thickness t is significantly smaller to the two other dimensions L_i ($t/L_i < 0.05$) [20]. Due to this small thickness-length ratio of the plates, through-thickness strains were neglected and conventional shell elements were used over continuum

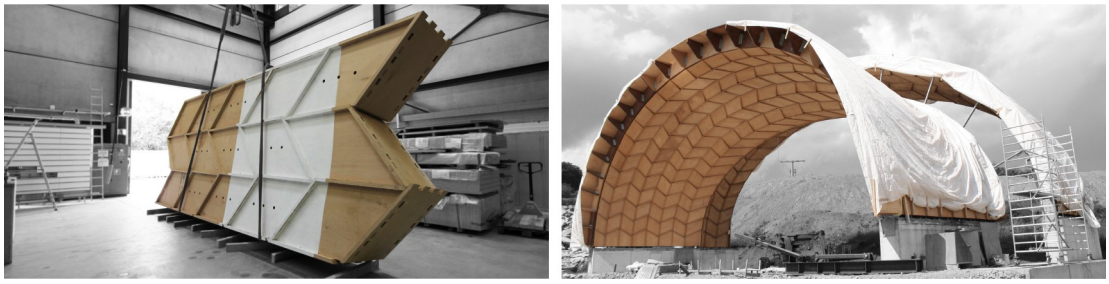

(a) Prototype 5×3 boxes, 6.88 m span (b) Prototype 1.5 arches, 24 m span

Fig. 3. Prototypes of double-layered timber plate structures scale 1:1 constructed.

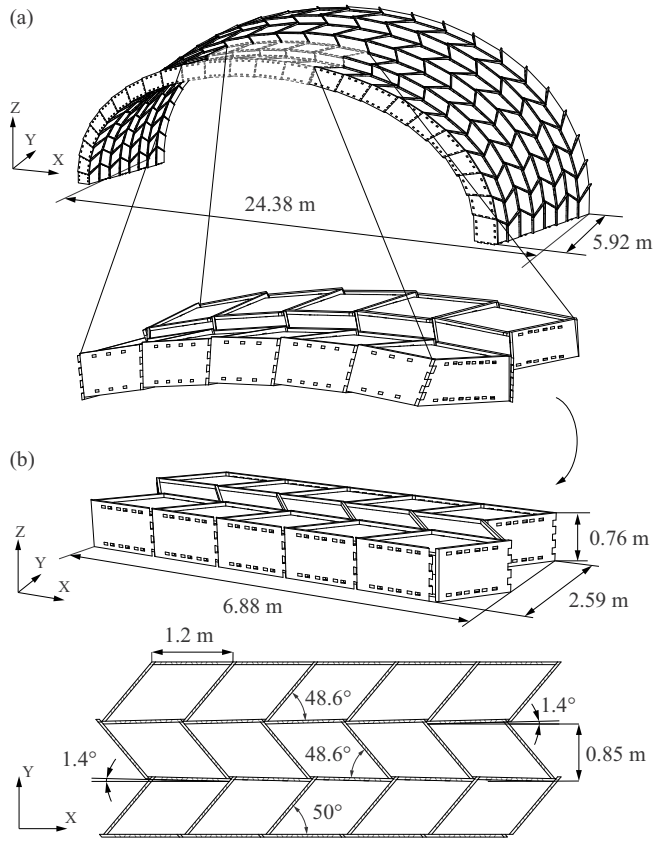

Fig. 4. Geometry of the 5×3 boxes prototype. (a) The boxes were extracted from a 24-meter span arch scale 1:1 and (b) their geometry was simplified to remove the curvature.

shell elements for all plates (horizontal $H_{i,1}$ and $H_{i,2}$ and vertical $V_{i,1}$ and $V_{i,2}$ in Fig. 2). Finite strain (also defined as large strain) S4R elements, 4-noded with 6 DOFs, were chosen for the mesh because of their robustness and as they are multi-purpose shell elements with hourglass control. The uniformly reduced integration helps to prevent shear and membrane locking [20]. Midsurfaces of the horizontal plates were extended to form closed boxes with the vertical plates. They were then reduced to introduce a small gap (0.5 mm) to implement the spring elements, modelling the connections, and the direction in which they act (see Fig. 5a).

For double-layered and double-curved timber plate shells, one issue of the geometry lies in the large dihedral angle φ between horizontal plates (close to 180° as shown in Fig. 5b), required for the curvature of the shell, and leading to a structure with tilted plates having a vertical plate in between with shared through-tenon connections. A spring model was developed since springs have been shown to be more rapidly computed than strip elements and the implementation of springs at the location of the joints is straightforward compared to strips elements which are difficult to obtain for tilted edges [14]. Equivalent elements such as springs have the advantages to be easily implemented, computationally efficient and easily applicable to other numerical software packages [21].

The semi-rigidity of through-tenon joints was introduced in the model by means of springs with stiffness values corresponding to the mechanical properties of the joints in the three translational and three rotational components of motion. All six components of motion were considered uncoupled. Due to the presence of vertical plates between neighbouring horizontal plates, springs were placed in a series on both sides of the vertical plates. Therefore, spring stiffness values k_i for each component of motion i had to be doubled:

$$k_i = \frac{1}{k_{i,1}} + \frac{1}{k_{i,2}} \quad (1)$$

$$k_{i,1} = k_{i,2} = 2 \cdot k_i \quad (2)$$

In previous research, discrete nodes were connected either by a single spring at the edges of the tenons [3] or by springs distributed along the length of the tenons [14,16] (see Fig. 5c). In this model, a kinematic coupling with all components of motion constrained was applied between the edge corresponding to the location of the joint and its midpoint (see Fig. 5d), as used by Sejkot et al. [22]. This edge-to-midpoint coupling prevents peak values at discrete points and is equivalent to an infinite number of discrete springs distributed along the edge. In order to identify the edges to be coupled and connected by spring elements, the surface of the plates was partitioned in order to identify the position of the joints in the CAD-FEM exchange geometry.

Dovetail joints connecting vertical plates along their shared edge were considered as rigid connections since the interlocking of the plates blocks the rotation at this connection. Vertical plates connected to each other were imported as one individual part.

At this stage, sources of modelling uncertainties can be linked to the mesh element type, mesh density and numerical solution procedure with convergence tolerances. A mesh convergence study was therefore carried out to assess the reliability of the results. Mesh seed sizes varying from 20 to 50 mm with steps of 10 mm and from 5 to 20 mm with steps of 2.5 mm were computed. A refined meshing strategy was also adopted to decrease the computation time of the numerical model. To achieve this mesh refinement strategy, plates were partitioned to have a finer mesh at the vicinity of the joints and a coarser mesh away from these regions (see Fig. 6).

5.1.2. Automatic generation of the CAD-FEM exchange geometry

The generation of the CAD-FEM exchange geometry defined in subsection 5.1.1 was implemented in the existing CAD plugin developed for double-layered and double-curved timber plate shells [6]. In this existing tool, two main classes called *box* and *plate* are defined and all boxes are composed of four plates: one top, one bottom and two side plates (see Fig. 7). These data structures include indexing, adjacency

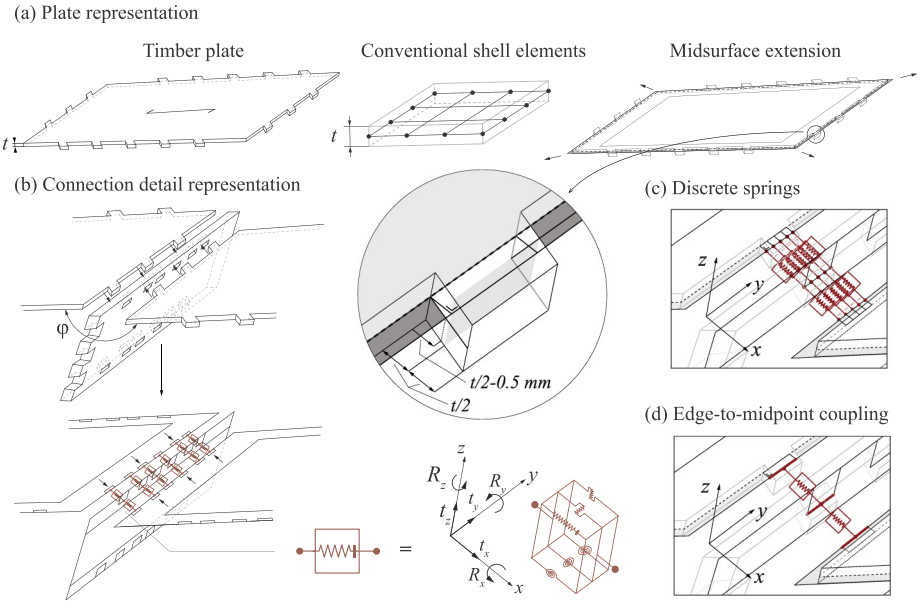

Fig. 5. Schematic representation of the numerical model for timber plates and MTSJ-TT connections. Midsurfaces of timber plates are modelled as conventional shell elements, extending the midsurface by $t/2$-0.5 mm to leave a small gap between the mid surface of the vertical panel, located at $t/2$. For the connections, springs with 6 components of motion (3 translational and 3 rotational) are implemented.

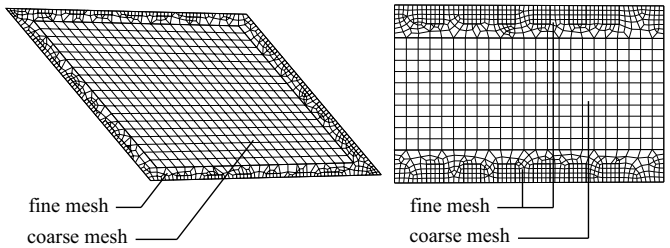

Fig. 6. Refined mesh strategy: horizontal and vertical plates were partitioned to have a finer mesh at the vicinity of the joints and a coarser mesh away from these regions.

properties, base plane and additional information helping the iteration over a collection of box components, while computing joinery between neighbouring box plates [6]. The same discretization method for the segmented timber shell system was used for the FEM geometry. However, the detailing phase differed depending on fabrication requirements and structural analysis application.

As a consequence, while the first model consisted of two polylines per plate, the CAD plugin was modified to represent the FEM geometry by four point outlines connected with line segments. In order to apply a refined meshing strategy, each outline was divided in subparts: outer outline and inner curve form an area for fine mesh, whereas the inner curve is only used for a coarser mesh. Joinery areas were represented as a series of rectangular elements perpendicular to each edge.

Plane-plane and line-plane intersection methods were applied in the proposed geometrical method. The procedure used to compute the FEM contour geometry each plate is illustrated in Fig. 8. All planes P_j from box B_i were derived from base mesh edge direction and normal. Top and bottom contours were obtained by retrieving the lines $L_{j\,j+1}$ at the intersection between the planes P_j and P_{j+1} and subsequently intersecting them with top and bottom planes P_T and P_B (see Fig. 8a). In the same manner, side plate contours were computed by retrieving the lines L_{0T}, L_{2T}, L_{0B} and L_{2B} at the intersection between the planes P_0, P_2, P_T and P_B and subsequently intersecting them with the side plane P_3; the operation was repeated for P_0 (see Fig. 8b). Finally, outlines for coarse mesh were obtained by offsetting neighbour planes in the direction of their normal and intersecting them with a base plane (see Fig. 8c). This geometrical operation is valid when angles between planes are not close to 180°; otherwise, a bisector plane must be added for computing the outline.

In the design model, the geometry of each tenon is characterized by three Bryant angles defining the insertion vector; however, in the FEM geometry, connections can be simplified to orthogonal shapes. Joinery

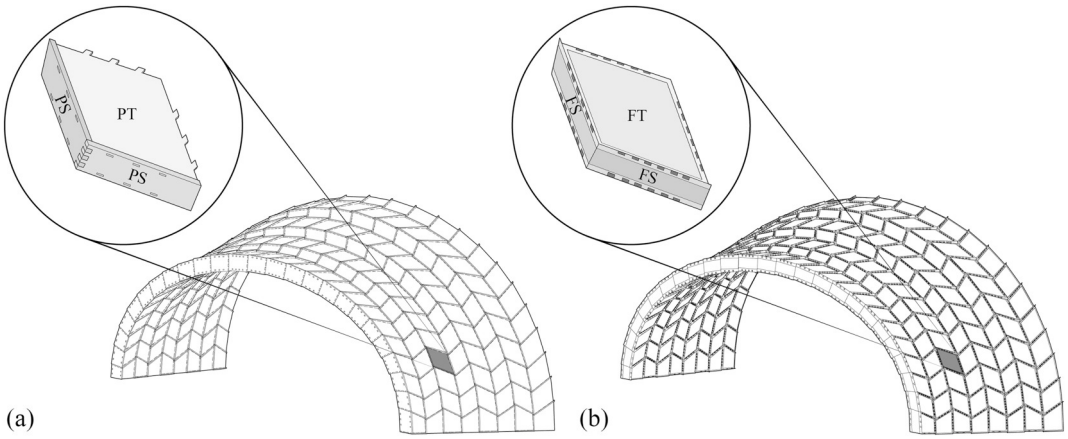

Fig. 7. (a) Design geometry, represented as a set of 4 plates: two top plates - 2 x PT and two side plates - 2 x PS; each of the plate consists of 2 polylines for CNC cutting (b) FEM geometry, represented as 4 surfaces that contains joinery elements, as well as fine and coarse subdivision areas.

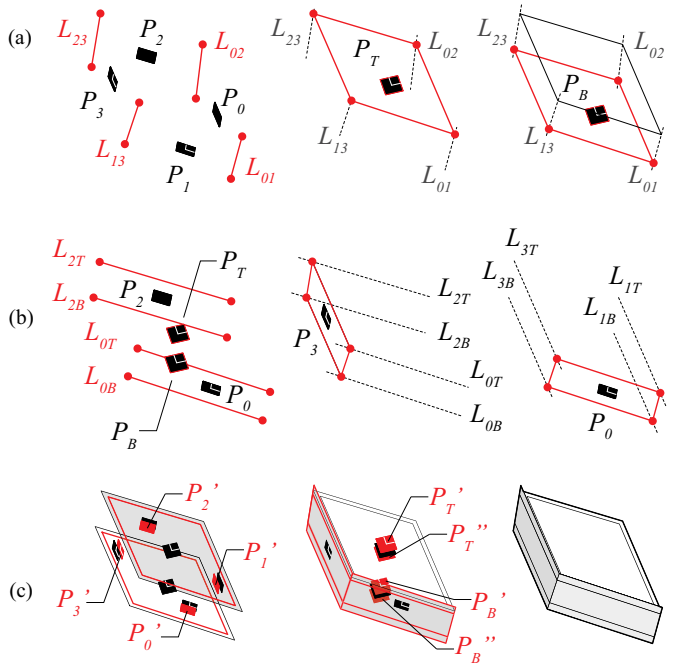

Fig. 8. Contour modelling steps using plane-plane and line-plane intersection methods for (a) top and bottom contours (b) side contours (c) offset of outlines for coarse and fine mesh areas.

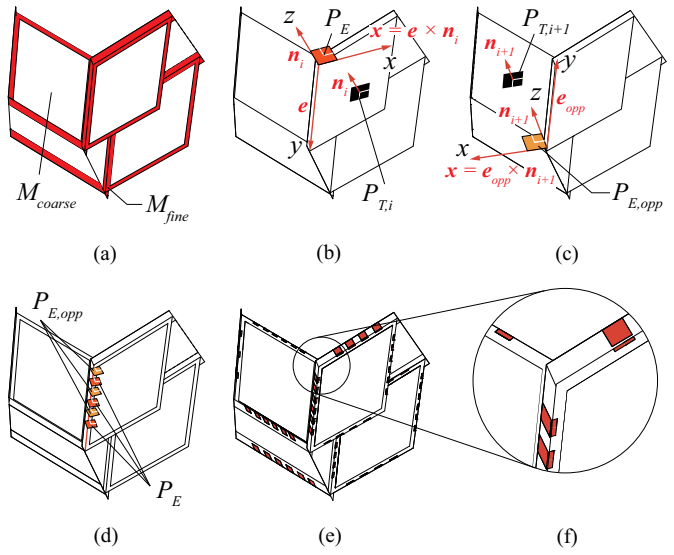

Fig. 9. Joinery modelling steps: (a) joinery zones are located in the fine mesh area M_{fine} (b)–(c) planes P_E and $P_{E,opp}$, used to compute the joinery areas of edge E and opposite edge E_{opp} respectively, are the planes xz (d) planes P_E and $P_{E,opp}$ are copied along the edges E and E_{opp} (e)–(f) outlines are cut by planes P_E and $P_{E,opp}$ to get rectilinear elements.

areas were therefore represented by a set of interpolated rectangles perpendicular to an edge and computed using line-plane intersections, as illustrated in Fig. 9. The coarse and fine meshing areas of each box, M_{coarse} and M_{fine} respectively, were first identified since the joinery areas are located in M_{fine} (see Fig. 9a). The planes P_E and $P_{E,opp}$ were used to compute the joinery areas of edge E and opposite edge E_{opp} respectively. They were defined as the planes xz, with the local x-axis determined by the cross product between the edge vector $\boldsymbol{e}/\boldsymbol{e}_{opp}$, of the edge E/E_{opp}, and the normal of the adjacent plate plane $\boldsymbol{n}_i/\boldsymbol{n}_{i+1}$, corresponding to the y and z-axis respectively (see Fig. 9b–c). The planes P_E and $P_{E,opp}$ were then copied along the edges E and E_{opp} (see Fig. 9d). Rectilinear elements were then created to identify the joints using plane-line intersection (see Fig. 9e–f). The height of the rectangles of the current plate was set slightly higher (1 mm) than the ones of the adjacent plate in order to identify the direction of the tenons in the FE model.

In the design model, the side plates of each box are connected by dovetail joints, whereas in the FE model, side surfaces were connected by the same edge (FS-FS common edge in Fig. 7) according to the defined FE model.

Finally, the geometry was returned to the CAD interface and prepared for export to the FEA software.

5.1.3. Automatic generation of the FE model

For structures with a large number of joints and unique shaped plates, a manual implementation of all parts of the structures and their connections in the FEA software would be too tedious. Consequently, a custom code in Python programming language was developed to generate the model from the CAD geometry exported to SAT files. The FE model was generated in the FEA software Abaqus™ using the Abaqus Scripting Interface. It was chosen as the geometry can be imported directly from a CAD software. However, the same principles can be applied to other platforms. In the CAD software used, in this case Rhino®, all boxes are numbered and organized; however, their importation into Abaqus™ is not. An algorithm was thus implemented to connect all plates together. The model was generated using the following steps, illustrated in Fig. 10:

1. The CAD-FEM exchange geometry was imported from SAT files for horizontal plates from both layers and for vertical plates. All plates were imported as individual parts, multiplying all lengths by a scale factor between the CAD software geometry (in this case in mm) and the FEA software using the SI units (i.e. Newtons, Pascals, kilograms, seconds and meters).
2. Material properties and section properties were assigned to all parts located within a defined bounding box. The material orientation of the plates was defined using the discrete method of orientation of Abaqus™ with the normal axis direction in the z-direction of each plate face and the primary axis direction x defined by the vector (1,0,0).
3. A coarse mesh was generated on each part located within the bounding box with defined seed size and element properties.
4. Potential edges corresponding to the location of the tenons were identified. These edges have a minimum and maximum possible length and are located on the outline of the parallelogram for horizontal plates and inside of the polygon for vertical plates. The identification of these edges, the coordinates of their centre point and the direction of the tenon were stored in two lists for horizontal and vertical plates respectively.
5. The edges were partitioned at their midpoint, suppressing the coarse mesh around the plates.
6. The mesh was regenerated with a refined seed size or with the same coarse seed size, depending on whether a refined meshing strategy was adopted or not.
7. Dependent part instances were created and assembled to form the whole geometry. As opposed to their independent counterparts, dependent instances refer to the original geometry of the parts imported; operations such as meshing and partitioning are performed on individual parts and not on instances.
8. Corresponding centre vertices from the two lists created were found and pairs were stored in a new list. Reference points were created for each centre point that was found to have a corresponding centre point and kinematic couplings were applied to the reference points and their edges.
9. Finally, springs were built between the pairs of vertices to connect horizontal and vertical plates.

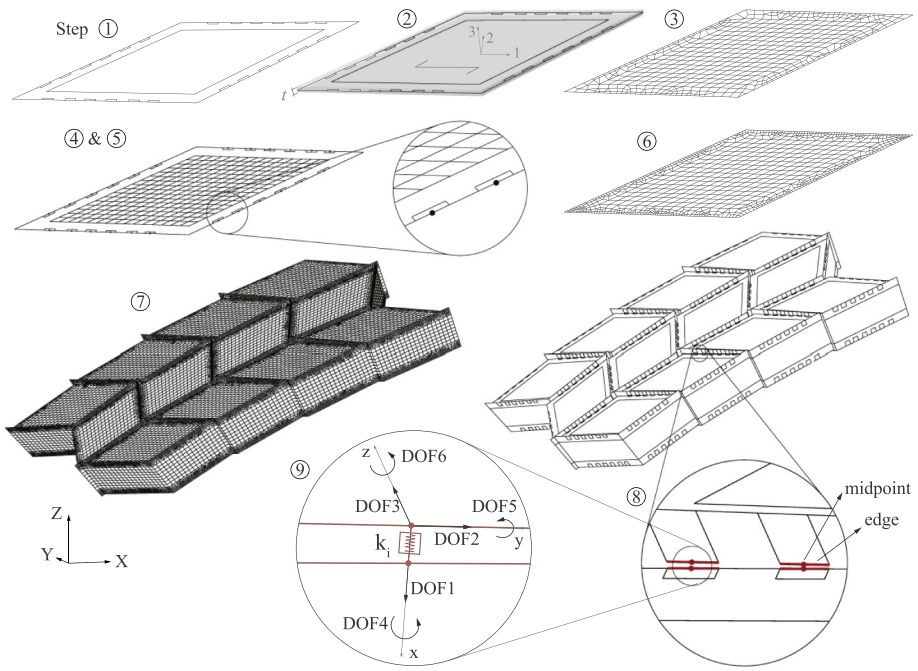

Fig. 10. Steps for the generation of the FE model in the FEA software.

5.2. Results

5.2.1. Automatic generation of the numerical model

The aim of an automated generation from CAD to FEM geometry was to avoid a manual process of transforming a large amount of plate elements to the defined exchange geometry. As a result, automation helped in decreasing the processing time of an initial manual generation of the FEM geometry, both time-consuming and containing user errors such as floating-point errors. Moreover, it allowed the application of the same code to a set of arches (see Fig. 11).

The numerical model was successfully generated from the CAD-FEM exchange geometry for both small-scale prototype (15 boxes) and large-scale arch (200 boxes). Table 1 presents the total number of variables and the minimum memory required (corresponding to the maximum amount of memory allocated by the analysis required to keep critical scratch data in memory [20]) for a small-scale prototype made of 5×3 boxes and a full-scale arch of 24-meter span.

Table 2 presents the time taken for each step described in subsection 5.1.3. Vertical panels were imported as joined parts since it was shown that the implementation of tie constraints between singular vertical panels drastically increases the model generation time. It is apparent that the time consuming step is step 6, corresponding to the regeneration of the mesh.

Table 1
Size-related parameters of small- and large-scale prototypes composed of 15 and 200 boxes respectively.

Parameter	15 Boxes	200 Boxes
Total number of variables	377 562	4 314 636
Min. memory required [Mb]	150	1 715

5.2.2. Mesh convergence study and refinement strategy

Fig. 12 presents the results of the mesh convergence study, which was carried out on the 5×3 prototype considering rigid beam connectors under a total load of 50 kN, which corresponds approximately

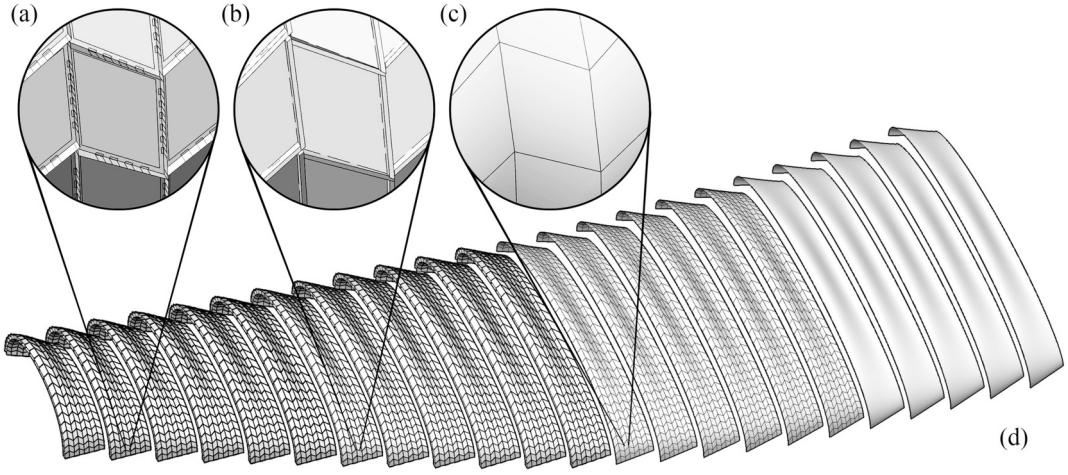

Fig. 11. Application of the same code generating the CAD-FEM exchange geometry to a set of arches (a) FEM geometry, (b) design geometry, (c) mesh subdivision and (d) design target surface.

Table 2
Time of each step of the generation of the FE model for small- and large-scale structures.

Step	Description	Time[a] for 15 boxes	Time[a] for 200 boxes
1	Importation of the parts	3.3 s	42.3 s
2	Material and properties assignment	0.4 s	2.5 s
3	Coarse mesh generation	5.7 s	55.1 s
4	Identification of the connections	34.8 s	4.5 min
5	Partitioning of edges	17.4 s	3.8 min
6	Mesh refinement generation	3.7 min	42.8 min
7	Assembly of the instances	0.1 s	7.0 s
8	Edge-to-midpoint coupling	4.1 s	2.3 min
9	Generation of the springs	45.8 s	5.3 min
	Total generation of the FE model	5.6 min	64.2 min

[a] Time obtained using a Lenovo Intel®CoreTM i7-4800MQ CPU @ 2.7 GHz with 16 GB of RAM.

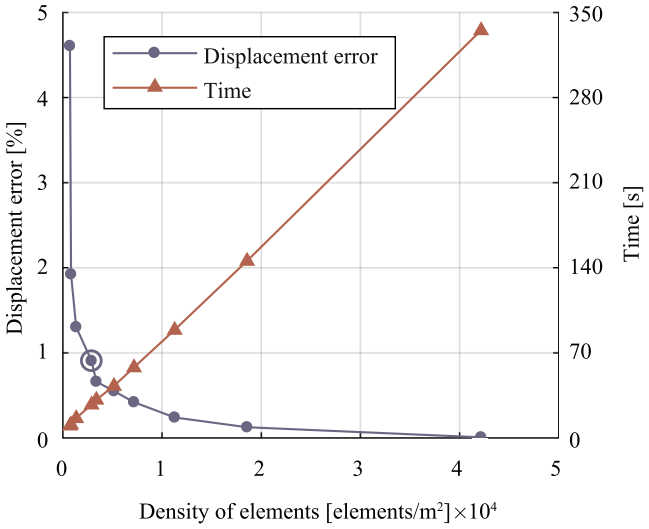

Fig. 12. Mesh convergence with respect to maximum vertical displacements results. A seed size of 20 mm (marked with a circle), leading to a relative error with respect to the displacement for the lowest seed size of 5 mm below 1%, was chosen.

to the maximum allowable displacement for serviceability limit state [16]. The density of elements corresponds to the number of elements per square meter. Results were compared considering computation time of the numerical model as well as vertical displacements. A seed size of 20 mm, leading to a relative error with respect to the displacement for the lower seed size of 5 mm below 1%, was chosen.

A mesh refinement study was then performed in order to decrease the computation time for the chosen seed size of 20 mm. In fact, since strains are concentrated at the location of the joints, a local mesh refinement was applied around the edges of the panels and larger elements were used away from these regions of interest. While using fine elements of 20 mm around the edges, coarser elements of 50 mm were used to reduce the computation time by 50% without significantly (< 0.4% difference) changing the results compared to a uniform mesh of 20 mm.

6. Structural analysis(Step 2)

In Section 5, corresponding to the first step of the design framework, the FE model was successfully generated for a series of double-layered double-curved timber plate shells. Consequently, structural analysis investigations were performed and the numerical model was assessed by comparing its results to experimental tests.

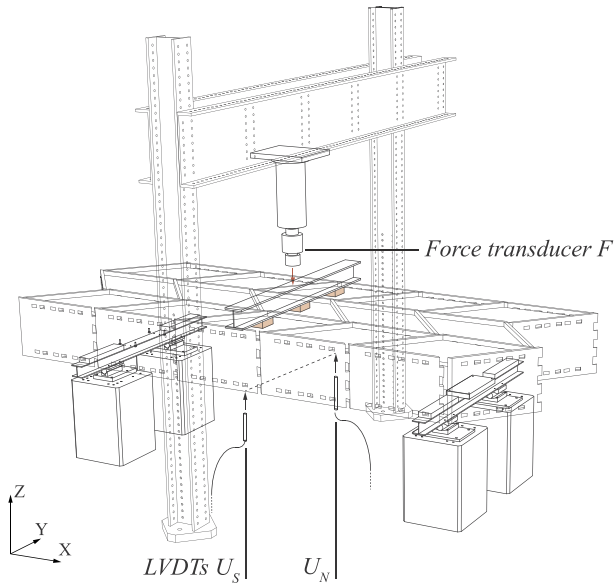

Fig. 13. Test setup and measurement instrumentation.

6.1. Methodology

Since previous research has shown that the mechanical behaviour of the joints highly influences the mechanical behaviour of the structures, the influence of the semi-rigidity of the springs modelling the connections was first investigated for each component of motion. In this section, sources of modelling uncertainties can be linked to the material model, the stiffness and modelling of the connections and the load and boundary conditions.

6.1.1. Experimental setup

In previous research, three-point bending tests have already been performed on two specimens of a prototype made of 5 × 3 boxes [16]. Because of the large dispersion of the results obtained, one additional test was carried out using the same test setup illustrated in Fig. 13. Load was applied through a hydraulic jack on the three top panels at midspan of the prototypes, using a beam to distribute the loads. Each prototype was fixed on steel profiles through timber blocks and the profiles themselves were fixed on rotulas fixed on four concrete blocks. Boundary conditions were pinned on one side of the prototype and rolled on the other side (see Fig. 14). The prototypes were monitored with a pair of linear variable differential transformers (LVDTs) placed on each side of the specimens at midspan to measure the vertical displacements of the vertical panels, and with a force transducer on the hydraulic jack.

6.1.2. Material model

Orthotropic material properties of each panel were implemented considering a single orthotropic layer with a defined local orientation for each plate. Material properties were considered linear elastic, such that the analysis was limited to linear kinematics, with mean values of elastic properties presented in Table 3. Poisson ratio values, not provided by the manufacturer, were retrieved from literature for beech [23]. Material, geometric and contact nonlinearities were not considered.

6.1.3. Semi-rigidity of the connections

The influence of each of the components of motion (3 translations and 3 rotations) of the spring element was investigated by comparing a model with rigid connections for all components and models with each

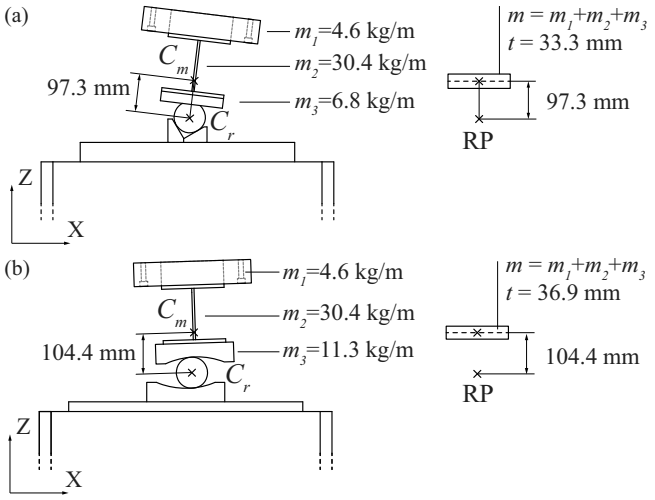

Fig. 14. Modelling of the (a) pinned and (b) roller supports.

Table 3
Elastic properties used for orthotropic material model of 40 mm thick BauBuche Q panels [19,23].

Property	Symbol	Value	Unit
Elastic modulus 11	E_{11}	13 200	N/mm^2
Elastic modulus 22	E_{22}	2200	N/mm^2
Elastic modulus 33	E_{33}	2200	N/mm^2
Shear modulus 12	G_{12}	820	N/mm^2
Shear modulus 13	G_{13}	430	N/mm^2
Shear modulus 23	G_{23}	430	N/mm^2
Poisson's ratio 12	ν_{12}	0.365	–
Poisson's ratio 13	ν_{13}	0.464	–
Poisson's ratio 23	ν_{23}	0.726	–
Density	ρ_{mean}	800	kg/m^3

of the 6 components of motion individually hinged. For components with an influence higher than 10% on the vertical displacements, values obtained from experimental tests were implemented.

6.1.4. Load and boundary conditions

Three steps of loading were defined in the model. In the first one, gravity load was implemented on the whole model. In the second one, the initial weight of the 230 × 230 mm wooden blocks and the load distributing beam was simulated by pressure load on 230 × 230 mm areas on the top plates located at midspan. Finally, the load was applied on the same areas to simulate the loading of the hydraulic jack.

Regarding the boundary conditions, the same modelling approach as presented in Stitic et al. [14] was used (see Fig. 14). In fact, when the structure is loaded, supports rotate around the *Y*-axis and the centre of mass is therefore not aligned to the centre of rotation of the steel rollers, resulting in nonlinear secondary moment effects [14]. Supports were therefore represented by 2.7-meter long and 0.16-meter wide steel plates with equivalent weight and distance to the centre of rotation as the actual setup. They were defined as rigid bodies associated with the corresponding centre of rotation defined as a reference point *RP*. Boundary conditions were applied to the reference points with free rotation along the global *Y*-axis for both supports and additional free translation along the global *X*-axis for the rolled support. Coupling constraints were assigned to the regions of the structure resting on the supports with corresponding reference points as control points.

6.2. Results

6.2.1. Semi-rigidity of the connections

As presented in Fig. 15, components 1 and 2 were shown to have a high influence on the vertical displacement of the structure (> 500%). The maximum displacement obtained when the component 3 was hinged gave an infinite vertical displacement (> 10^7 mm). This is explained by the fact that it represents the motion in the *z*-direction; if this component is completely hinged, the vertical displacement is not blocked and very high values are thus obtained. A maximum value of 600 mm, corresponding to the height of the boxes was therefore considered (> 5000%). Regarding rotations, component 5 highly influenced the vertical displacements of the structure (> 70%) compared to components 4 and 6 which had a limited influence (< 6%). For the final model, the semi-rigidity of the connections for the components 1, 2, 3 and 5 were thus tested.

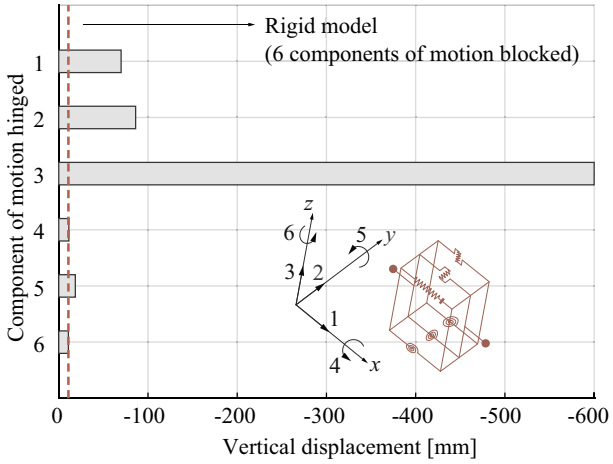

Fig. 15. Influence of each component of motion on the vertical displacements. The dotted line represents the results obtained when all 6 components were blocked. The bars represent the displacements obtained when each of the 6 components were individually hinged while keeping the 5 remaining components rigid.

Spring stiffness k_i used for each of the components of motion are presented in Table 4. Values of k_1, k_2 and k_3 were retrieved from experimental tests performed on small specimens [24]. For k_1, a nonlinear spring was implemented using Abaqus™ bushing connectors, with a high value of 10^9 N/mm in compression, to be considered rigid, and the axial stiffness in tension. The test setup used for the axial stiffness k_1 is presented in [25]. For the in-plane shear stiffness k_2, the setup presented in [26] was used. A similar setup was used to retrieve the stiffness k_3 [24]. For the rotational stiffness k_5, an existing experimental setup developed by Roche [27] was used. Bending tests performed are presented in Appendix A. According to investigations on the influence of each spring component on the model, rotations around *x* and *z* were considered rigid and a high value of 10^{15} N·mm/° was thus set for k_4 and k_6.

6.2.2. Finite element model for small-scale prototypes

Fig. 16a presents the results of the experimental tests performed on the three 5 × 3 boxes specimens which were tested. Results of the additional test on a third specimen were between previous results

Table 4
Values of springs' stiffness used in the FE model for each of the 6 components of motion [24-26,14].

Symbol	Component	Value	Units
k_1	Translation *x*	416.81	N/mm
k_2	Translation *y*	15 009.24	N/mm
k_3	Translation *z*	9 489.04	N/mm
k_4	Rotation around *x*	10^{15}	N·mm/°
k_5	Rotation around *y*	170 190.41	N·mm/°
k_6	Rotation around *z*	10^{15}	N·mm/°

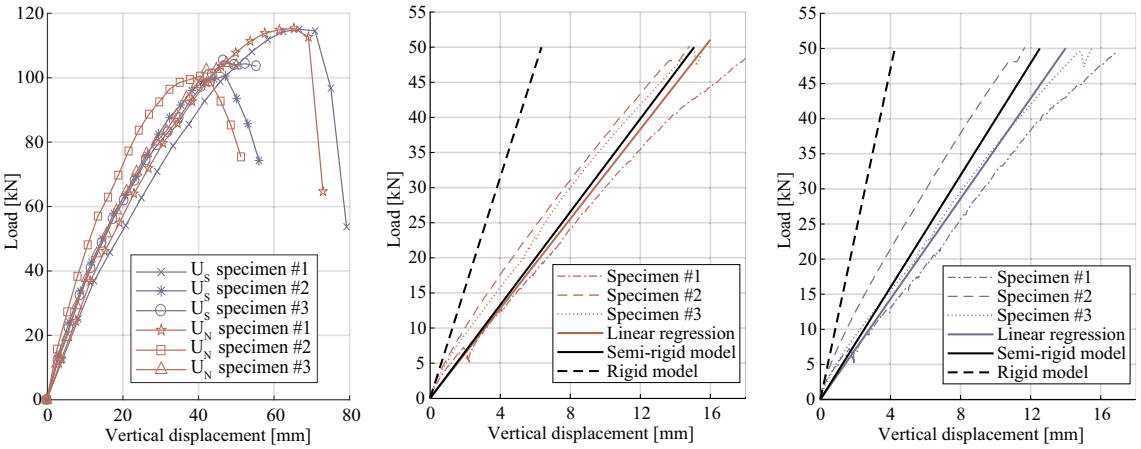

(a) Experimental tests (b) LDVT U_N (c) LDVT U_S

Fig. 16. Load vs. midspan deflection: (a) Experimental results for the three specimens tested and (b)–(c) comparison between linear regression of experimental tests and numerical results for 50 kN load, which approximately corresponds to the maximum allowable displacement for SLS for the north and the south side respectively.

obtained [16]. The maximum additional load at failure was of 107.23 kN on average with a coefficient of variation of the maximum additional load at failure $c_{v,Fmax}$ of 6.95%, with the coefficient of variation c_v defined as:

$$c_v = \frac{\sigma}{\mu} \tag{3}$$

where σ is the standard deviation and μ the average.

To compare experimental to numerical results, the maximum load considered was about 50 kN, which corresponds approximately to the maximum allowable displacement for serviceability limit state, to limit the study to linear kinematics. Moreover, initial displacements due to gravity and due to the weight of the distributing steel beam and the wooden blocks were subtracted from the displacements obtained in the subsequent loading steps. In fact, experimental measurements were taken after the disposition of the specimen on the supports and of loading elements on the specimen. Propagated effects of gravity and initial loading could thus be considered in the model.

Fig. 16 b and c present the results of the proposed spring model compared to the linear regression of experimental tests in the linear elastic part of loading for the north and the south side of the prototype respectively. A large dispersion in the results can still be observed. In fact, the coefficient of variation of the stiffness $c_{v,k}$ was found to be of 16.63%.

Results of this model were compared to a model with a high stiffness value for all components of motion of the springs (rigid model). The semi-rigid model was shown to be 4 and 12% more rigid compared to the experimental tests for the north and the south side respectively. In comparison, a rigid model was 146 and 230% more rigid for the north and the south side respectively.

At the beginning of the test, for a load under 5 kN, a very stiff behaviour can be observed. This can be attributed to the initial stiffness of the connections when all faces are set in contact. This corresponds to a very high stiffness due to the full interlocking between the tenon and the mortise.

7. Conclusions

This paper presents a method to automate the generation of an FE model for the structural analysis of timber plate structures with a large number of wood-wood connections, taking the example of double-layered and double-curved timber plate shells.

In the design framework presented, the existing CAD plugin was modified to generate a CAD-FEM geometry, made of surfaces partitioned at the position of the joints, which could be directly imported in the FEA software, in this case Abaqus™.

A numerical model using springs with an edge-to-midpoint coupling to model the semi-rigidity of wood-wood connections was developed. It was successfully generated in the FEA software using a custom developed Python code, avoiding a tedious and time-consuming manual implementation. Another advantage over a manual generation is that it prevents human errors. Nonlinear springs were used to model the axial stiffness of the connections, whereas linear springs were used for the other components.

Semi-rigidity of the connections in translation as well as in rotation was shown to be of importance. Vertical displacements of the numerical model were shown to be in good agreement with three-point bending tests performed on three small-scale specimens, using the values of semi-rigidity from experimental tests on wood-wood connections. Furthermore, taking the semi-rigidity of the joints in the model was shown to be essential since the semi-rigid model was shown to be 8% stiffer than experimental tests, whereas a rigid model was 188% stiffer in average. Introducing semi-rigidity for rotational components of motion about x and z would lead to a more flexible behaviour of the structure, such that the results could be considered as on the safe side.

The limitations of the model can be linked to friction and indirect compression zones, both neglected in the model. Moreover, a stiffer behaviour was observed at the beginning of the test. This can be attributed to the nonlinear behaviour of the connections, which would have to be implemented in the model to increase its accuracy in the first loading steps. Coupling terms between the components of motion of the springs were also discarded. Therefore, further studies on the mechanical behaviour of wood-wood connections, such as carried for the moment resisting behaviour by Roche [27], could help improve the global model.

The model was successfully generated for large-scale structures; however, numerical results were not compared to experimental tests for those structures.

Although the model was applied to a specific type of structure, it is straightforward and can thus be applicable to various plate structures using wood-wood connections. Consequently, the presented work has the potential to enhance exchanges between geometry generation and structural analysis, necessary to perform structural optimization studies.

Declaration of Competing Interest

None.

Acknowledgements

This research was supported by the NCCR Digital Fabrication, funded by the Swiss National Science Foundation (NCCR Digital Fabrication Agreement #51NF40-141853). The authors would like to thank the technicians of the Structural Engineering Group of the École Polytechnique Fédérale de Lausanne for their assistance in the experimental tests and Annen SA for the fabrication of the small-scale prototypes tested.

Appendix A. Bending tests

Bending tests were performed on wood-wood connections in order to retrieve the rotational stiffness to implement in the finite element model of small- and large-scale double-layered timber plate shells. They were carried out on a series of seven specimens made of two-panel assemblies connected with one through-tenon connection with the geometry presented in Fig. A.1.

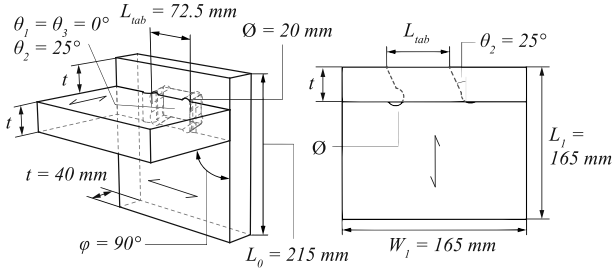

Fig. A.1. MTSJ through-tenon connection details of the specimens tested: perspective view (left) and top view (right). Length of all tabs was fixed to 72.5 mm with Bryant angles $\theta_1 = \theta_3 = 0°$ and $\theta_2 = 25°$.

The bending test setup developed by Roche [27] and illustrated in Fig. A.2 was used. Four load cells ① were fixed on each panel; for the panel with slots, these load cells were mounted on a rigid support while for the panel with tenon, they were fixed to a level arm ②, itself connected to a 20 kN load cylinder. Two inclinometers ③ were fixed to the panel with tenon to measure the rotation of the sample. Specimens were tested in closing as through-tenon connections have been shown to present a symmetrical behavior in opening and closing [13].

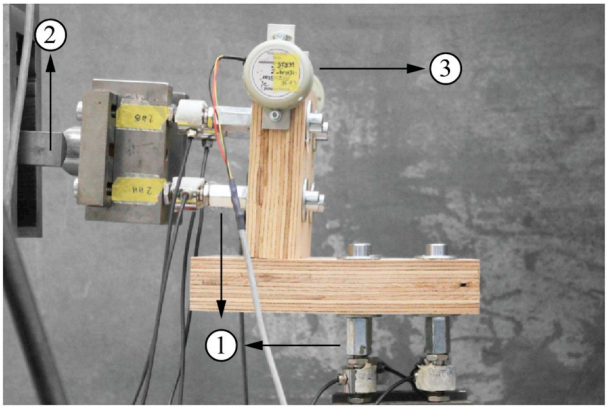

Fig. A.2. Bending setup developed by Roche [27]: four load cells ① were fixed on each panel; for the panel with slot, these load cells were mounted on a rigid support while for the panel with tenon, they were fixed to a level arm ②, itself connected to a 20 kN load cylinder. Two inclinometers ③ were fixed to the panel with tenon to measure the rotation of the sample in closing.

Fig. A.3a presents the moment-rotation curves obtained for the seven specimens tested. The maximum average moment applied M_{max} was 1067.0 kN·mm. Fig. A.3b presents the moment-rotation curves in the linear range between 10 and 40% of M_{max} from which the stiffness was retrieved. A linear regression led to an average stiffness of 170.19 kN·mm/°.

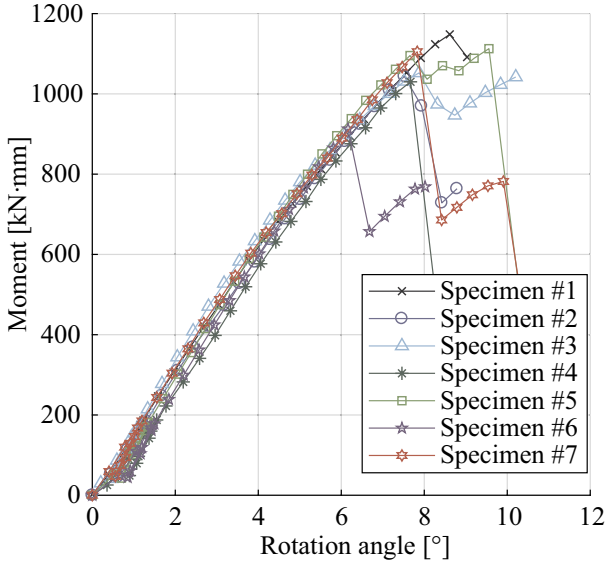

(a)

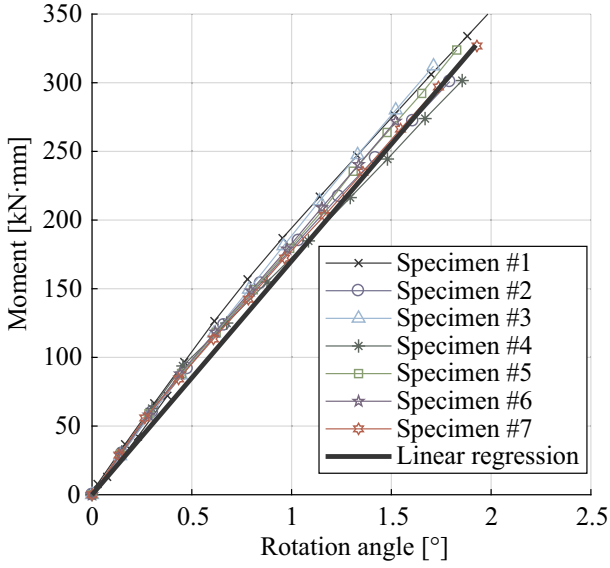

(b)

Fig. A.3. (a) Moment-rotation curves and (b) linear range between 10 and 40% of M_{max}.

References

[1] C. Robeller, Integral Mechanical Attachment for Timber Folded Plate Structures, Ph.D. thesis École Polytechnique Fédérale de Lausanne, 2015, https://doi.org/10.5075/epfl-thesis-6564.

[2] R. La Magna, M. Gabler, S. Reichert, T. Schwinn, F. Waimer, A. Menges, J. Knippers, From nature to fabrication: biomimetic design principles for the production of complex spatial structures, Int. J. Space Struct. 28 (2013) 27–39, https://doi.org/10.1260/0266-3511.28.1.27.

[3] J.-M. Li, J. Knippers, Segmental timber plate shell for the Landesgartenschau Exhibition Hall in Schwäbisch Gmünd - the application of finger joints in plate structures, Int. J. Space Struct. 30 (2) (2015) 123–140, https://doi.org/10.1260/0266-3511.30.2.123.

[4] C. Robeller, J. Gamerro, Y. Weinand, Théâtre Vidy Lausanne - A double-layered timber folded plate structure, J. Int. Assoc. Shell Spat. Struct. 58 (2017) 295–314, https://doi.org/10.20898/j.iass.2017.194.864.

[5] E.M. Meghlat, M. Oudjene, H.H. Ait-Aider, J.-L. Batoz, A new approach to model nailed and screwed timber joints using the finite element method, Constr. Build. Mater. 41 (2013) 263–269, https://doi.org/10.1016/j.conbuildmat.2012.11.068.

[6] C. Robeller, M. Konakovic, M. Dedijer, M. Pauly, Y. Weinand, A double-layered timber plate shell - computational methods for assembly, prefabrication and structural design, in: S. Adriaenssens, F. Gramazio, M. Kohler, A. Menges, M. Pauly (Eds.), Advances in Architectural Geometry 2016, vdf Hochschulverlag AG, ETH Zürich, 2016, pp. 104–122, , https://doi.org/10.3218/3778-4_9.

[7] A. Menges, Manufacturing diversity, Archit. Des. 76 (2006) 70–77, https://doi.org/10.1002/ad.242.

[8] F. Scheurer, C. Schindler, M. Braach, From design to production: three complex structures materialised in wood, in: C. Soddu (Ed.), 6th International Conference Generative Art 2005 Milan, 2005, p. 403412 https://doi.org/20.500.11850/66706.

[9] F. Kaltenbach, Teaching by doing - a research pavilion in Stuttgart, Detail (English Edition) 2010 (6) (2010) 559–561 ISSN: 1614-4600.

[10] T. Schwinn, O.D. Krieg, A. Menges, Robotically fabricated wood plate morphologies, in: S. Brell-Çokcan, J. Braumann (Eds.), Rob | Arch 2012, Springer-Verlag, Wien, 2013, pp. 48–61, , https://doi.org/10.1007/978-3-7091-1465-0_4.

[11] P. Flores, Euler Angles, Bryant Angles, Euler Parameters, Concepts and Formulations for Spatial Multibody Dynamics, 1st Edition, Springer International Publishing, Cham, 2015, pp. 15–22, https://doi.org/10.1007/978-3-319-16190-7_4, Ch. 4.

[12] C. Robeller, A. Stitic, P. Mayencourt, Y. Weinand, Interlocking folded plate: integrated mechanical attachment for structural wood panels, in: P. Block, J. Knippers, N.J. Mitra, W. Wang (Eds.), Advances in Architectural Geometry 2014, Springer International Publishing, Cham, 2015, pp. 281–294, , https://doi.org/10.1007/978-3-319-11418-7_18.

[13] S. Roche, J. Gamerro, Y. Weinand, Multiple tab-and-slot joint: improvement of the rotational stiffness for the connection of thin structural wood panels, in: J. Eberhardsteiner, W. Winter, A. Fadai, M. Pöll (Eds.), WCTE 2016 World Conference on Timber Engineering e-book, TU Verlag, Vienna, 2016, pp. 1556–1564, , https://doi.org/10.5075/epfl-ibois-221012.
[14] A. Stitic, A.C. Nguyen, A.R. Rad, Y. Weinand, Numerical simulation of the semi-rigid behaviour of integrally attached timber folded surface structures, Buildings 9 (2) (2019) 55, https://doi.org/10.3390/buildings9020055.
[15] A. Bagger, Plate Shell Structures of Glass - Studies Leading to Guidelines for Structural Design, Ph.D. thesis Technical University of Denmark, 2010, http://orbit.dtu.dk/files/5475675/Anne%20Bagger_PhDthesis_April10_incl_cover.pdf.
[16] A.C. Nguyen, Y. Weinand, Development of a spring model for the structural analysis of a double-layered timber plate structure with through-tenon joints, WCTE 2018 World Conference on Timber Engineering CD-ROM Proceedings, 2018, pp. 1–7, , https://doi.org/10.5075/epfl-ibois-256749 Seoul, South Korea.
[17] M. Hirz, W. Dietrich, A. Gfrerrer, J. Lang, Integrated Computer-Aided Design in Automotive Development, Springer-Verlag, Berlin Heidelberg, 2013, https://doi.org/10.1007/978-3-642-11940-8.
[18] R. Pedreschi, D. Theodossopoulos, The double-curvature masonry vaults of Eladio Dieste, Proc. Inst. Civ. Eng. Struct. Build. 160 (1) (2007) 3–11, https://doi.org/10.1680/stbu.2007.160.1.3.
[19] H.J. Blaß, J. Streib, BauBuche Beech laminated veneer lumber - Design assistance for drafting and calculation in accordance with Eurocode 5, http://pollmeier.com/en/downloads/designmanual, (2017) , Accessed date: 17 May 2019.
[20] Abaqus 6.12 Online Documentation, http://abaqus.software.polimi.it/v6.12/index.html, (2012) , Accessed date: 17 May 2019.
[21] M. Berot, Modélisation simplifiée d'assemblages par éléments équivalents, Ph.D. thesis École Nationale Supérieure des Mines de Paris, 2009, http://pastel.archives-ouvertes.fr/tel-00443533/document , Accessed date: 17 May 2019.
[22] P. Sejkot, S. Ormarsson, J. Vessby, Numerical and experimental study of punched metal plate connection used for long-span pitched timber roof truss structure, WCTE 2018 World Conference on Timber Engineering CD-ROM Proceedings, (2018), pp. 1–8 Seoul, South Korea http://lnu.diva-portal.org/smash/get/diva2:1306811/FULLTEXT01.pdf , Accessed date: 26 June 2019.
[23] D. Guitard, Mécanique Du Matériau Bois et Composites, Cepaduès Editions, Toulouse, 1987 ISBN: 2-85428-152-7.
[24] A.C. Nguyen, A.R. Rad, Y. Weinand, Semi-Rigidity of Through-Tenon Joints under Tension and Shear Loads and Perpendicular-to-Grain Compression, (2019), https://doi.org/10.5075/epfl-IBOIS-265676.
[25] A.R. Rad, H. Burton, Y. Weinand, Performance assessment of through-tenon timber joints under tension loads, Constr. Build. Mater. 207 (2019) 706–721, https://doi.org/10.1016/j.conbuildmat.2019.02.112.
[26] A.R. Rad, Y. Weinand, H. Burton, Experimental push-out investigation on the in-plane force-deformation behavior of integrally-attached timber Through-Tenon joints, Constr. Build. Mater. 215 (2019) 925–940, https://doi.org/10.1016/j.conbuildmat.2019.04.156.
[27] S. Roche, Semi-Rigid Moment-Resisting Behavior of Multiple Tab-and-Slot Joint for Freeform Timber Plate Structures, Ph.D. thesis École Polytechnique Fédérale de Lausanne, 2017, https://doi.org/10.5075/epfl-thesis-8236.